Locus-Conserved Circular RNA cZNF292 Controls Endothelial Cell Flow Responses

Andreas W. Heumüller[1,2], Alisha N. Jones[3,4], André Mourão[3,4], Marius Klangwart[1], Chenyue Shi[5], Ilka Wittig[6,11], Ariane Fischer[1], Marion Muhly Reinholz[1], Giulia K. Buchmann[7], Christoph Dieterich[8], Michael Potente [5, ,9,10,11,12], Thomas Braun [5,11,12], Phillip Grote[1], Nicolas Jaé[1], Michael Sattler[3,4], Stefanie Dimmeler (*) [1,11,12]

[1] Institute of Cardiovascular Regeneration, Goethe University, Theodor Stern Kai 7, Frankfurt Germany. [2] Faculty for Biological Sciences, Goethe University, 60590 Frankfurt, Germany; [3] Institute of Structural Biology, Helmholtz Zentrum München Ingolstädter Landstr. 1, 85764 Neuherberg, Germany; [4]Biomolecular NMR and Center for Integrated Protein Science Munich at Department Chemie, Technical University of Munich, Lichtenbergstraße 4, 85747, Garching, Germany; [5] Max Planck Institute for Heart and Lung Research, Bad Nauheim, Germany; [6] Functional Proteomics, Institute for Cardiovascular Physiology, Goethe University, Theodor Stern Kai 7, Frankfurt Germany; [7]Institute for Cardiovascular Physiology, Goethe-University, Theodor-Stern Kai 7, 60590, Frankfurt Am Main, Germany;[8] Department of Cardiology, Angiology, and Pneumology, University Hospital Heidelberg; [9] Berlin Institute of Health at Charité – Universitätsmedizin Berlin, Berlin, Germany; [10] Max Delbrück Center for Molecular Medicine in the Helmholtz Association (MDC), Berlin, Germany; [11]German Center for Cardiovascular Research (DZHK); Frankfurt; Germany, and; [12] Cardio-Pulmonary Institute (CPI), Frankfurt; Germany.

***Running title*:** cZNF292 Controls Endothelial Cell Flow Response

Circulation Research

Subject Terms:
Cell Biology/Structural Biology
Vascular Biology

Address correspondence to:
Dr. Stefanie Dimmeler
Institute of Cardiovascular Regeneration, Goethe University
Theodor Stern Kai 7
60590 Frankfurt am Main
dimmeler@em.uni-frankfurt.de

ABSTRACT

Background: Circular RNAs (circRNAs) are generated by back-splicing of mostly mRNAs and are gaining increasing attention as a novel class of regulatory RNAs that control various cellular functions. However, their physiological roles and functional conservation *in vivo* are rarely addressed, given the inherent challenges of their genetic inactivation. Here we aimed to identify locus conserved circRNAs in mice and humans, which can be genetically deleted due to retained intronic elements not contained in the mRNA host gene to eventually address functional conservation.

Methods: Mechanistically, we identified the protein syndesmos (SDOS) to specifically interact with *cZNF292* in endothelial cells by RNA affinity purification and subsequent mass spectrometry analysis. Silencing of SDOS or its protein binding partner Syndecan-4, or mutation of the SDOS-*cZNF292* binding site, prevented laminar flow-induced cytoskeletal reorganisation thereby recapitulating *cZfp292* phenotypes.

Results: Combining published endothelial RNA sequencing datasets with circRNAs of the circATLAS databank, we identified locus-conserved circRNA retaining intronic elements between mice and humans. CRISPR/Cas9 mediated genetic depletion of the top expressed circRNA *cZfp292* resulted in an altered endothelial morphology and aberrant flow alignment in the aorta *in vivo.* Consistently, depletion of *cZNF292* in endothelial cells *in vitro* abolished laminar flow-induced alterations in cell orientation, paxillin localisation and focal adhesion organisation.

Conclusion: Together, our data reveal a hitherto unknown role of *cZNF292/cZfp292* in endothelial flow responses, which influences endothelial shape.

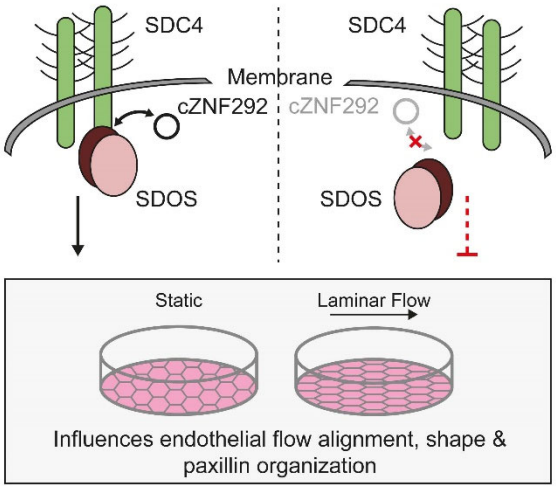

Non-standard abbreviations and acronyms	
Ago-HITS-CLIP	High-throughput sequencing of RNA isolated by crosslinking immunoprecipitation
circRNA	circular RNA
cZNF292	circular RNA of ZNF292
EMSA	electrophoretic mobility shift assay
HUVEC	Human umbilical vein endothelial cells
PXN	Paxillin
RIP	RNA immunoprecipiation
SDC4	Syndecan-4
SDOS	Syndesmos, NUDT16L1
ZNF292/Zfp292	Zinc finger protein 292

INTRODUCTION

Endothelial cells play a critical role in the maintenance of organ functions. Being located at the inner wall of the vessels, endothelial cells are exposed to diverse circulating stimuli and blood flow, which itself induces a variety of intracellular signaling cascades [1,2]. Impaired endothelial cell function is associated with various diseases, including atherosclerosis, thrombosis or hypertension, often preceding major vascular events such as stroke or myocardial infarction. Non-coding RNAs are increasingly recognized as crucial regulators of endothelial cell functions[3]. Circular RNAs (circRNAs) are a subset of non-coding RNAs generated by back-splicing of predominantly protein-coding exons. Different from canonical splicing, back-splicing ligates a downstream splice donor site with an upstream splice acceptor site, thereby generating covalently closed circular RNAs[4]. After the initial identification of various circRNA in endothelial cells[5], several have been functionally investigated *in vitro*. For example, cZNF292 silencing was shown to reduce angiogenic responses of cultured endothelial cells *in vitro*[5], whereas cHIPK3 silencing prevented retinal vascular dysfunction in diabetes[6]. However, their mechanism of action is often only poorly understood and evidence for a functional role employing genetic ablation models *in vivo* is rare[7,8]. This is mainly due to the difficulty to eliminate the specific circRNA without altering the levels of the linear host mRNA produced from the same gene. In the case of circRNA *Cdr1as*, it was possible to delete the entire locus since the linear mRNA was lowly expressed[7]. This deletion was shown to affect brain function[7]. Other studies mutated or deleted flanking regions to reduce circRNA biogenesis [8] or have used short hairpin RNAs to target the back splice site[9], however, such approaches often are confounded by off-target effects.

To circumvent these issues and understand the impact of circRNAs in vascular biology *in vivo*, we aimed to target circRNAs containing intronic sequences as identified in previous studies[10], with the perception that intros are not part of the mature mRNA of the host gene, and therefore can be targeted for selective circRNA deletion.

METHODS

Data Availability.
All of the data and information supporting the findings of this study are stated in the manuscript, the supplemental material, the Major Resource Table, or are available from the corresponding author upon request. RNA-sequencing data is publicly available at the GEO repository under the accession XXX and GSE107033. Mass spectrometry data is publicly available at the PRIDE repository under the accession XXX.

RNA Sequencing.
Data was either publicly available[5,11] or generated at the European Molecular Biology Laboratory (EMBL, Heidelberg, Germany) with paired-end 2 × 75 nucleotide reads. The removal of rRNA was performed with the Ribo-Zero Gold (Epicentre Biotechnologies, Madison, Wisconsin, USA; Cat# RS-122-2301) or NEBNext rRNA Depletion kit (New England Biolabs, Frankfurt, Germany; Cat# E6310L). The datasets (HUVEC RNaseR, HCMEC/HAOEC) were analysed as described previously[11].

RNA Affinity Purification.
RNA affinity purification was performed using native HUVEC lysates obtained after lysis in µl Buffer R (50 mM Tris HCl pH=8, 50 mM NaCl, 0.5% (v/v) NP-40, 0.1 mM $MgCl_2$ and 1x Protease Inhibitor Cocktail). Lysates were diluted to working concentration of RNase R buffer and linear RNA was partially degraded by incubation with RNase R for 10 min. For pulldown, 1 µl of 100 µM 2'O-Me biotinylated RNA-antisense probes (IDT) were added to the lysates and incubate over night with gently agitation. Probes were recovered using blocked Dynabeads MyOne Streptavidin-Beads C1 beads for 1 h a t room temperature after which beads were washed and samples were eluted by replacement with D-Biotin. Samples were submitted to 2/3 for analysis by mass-spectrometry and 1/3 was used for RNA analysis.

Electrophoretic Mobility Shift Assays.
Electrophoretic mobility shift assays were performed using 5 nM ^{32}P-labeled RNA incubated with increasing concentrations of SDOS protein (wildtype or mutant) in buffer containing 10 mM HEPES, 100 mM NaCl and 1 mM beta-mercaptoethanol. Reactions were run on a 0.7% agarose dissolved in 1X TBE. Gels were exposed for two hours on a GE-phosphor plate prior to scanning on a Typhoon 9000 imager. Band intensity was quantified using ImageJ, followed by fitting in Kaleidograph for determination of the dissociation constant with the Hill-equation. Errors indicated represent the error of fit. At least two biological replicates were run for each EMSA.

Laminar Flow Experiments.
Laminar flow experiments were performed using the Ibidi Perfusion System was used. A total of 2.5 *10^5 HUVECs were reseeded 24h after siRNA silencing or 48h after lentiviral overexpression to 0.4 Luer Ibidi µ-Slides and were allowed to attach for 3h. Cells were exposed to unidirectional laminar flow (12 dyn/cm², 40h) using the Ibidi Perfusion System following the suppliers' instructions. For static controls, cells were not exposed to flow and media was changed daily. Following, cells were washed once with PBS containing calcium and magnesium and fixed with 4% formaldehyde/PBS for 10 min at room temperature.

Immunofluorescence labelling.
Immunofluorescence labelling were performed after cells were reseeded 24h following siRNA silencing to fibronectin coated 4-well (1*10^5 HUVECs) or 8-well (4*10^4 HUVECs) chamber µ-slides (Ibidi) and cultured for an additional 24 h. Afterwards, cells were washed once with PBS, fixed with 4% formaldehyde/PBS for 10 min at room temperature, permeabilized with 0.1% TritonX-100 for 10 min at RT, blocked in 10% normal donkey serum and stained with primary antibodies in the blocking solution overnight at 4°C. Antibodies used for staining were as follows: PXN (abcam, ab32084, 1:200), Cd144

(BD, #555289, 1:50), CD31 (BD, #553370, 1:50), ERG (abcam). Cells were washed thrice with PBS containing 0.05% Tween-20 before incubation with fluorescent labelled secondary antibodies (1h, RT in PBS). F-Actin staining were performed with Phalloidin-488 (ThermoFisher Scientific) and included during the secondary antibody incubation at a dilution of 1:50. DAPI stainings were included during the secondary antibody incubation at a dilution of 1:200. Cells were mounted in Fluoromount-G and imaged using a NikonTie2 Eclipse microscope or Leica SP8 confocal microscope.

Lentiviral Overexpression.
Lentiviral overexpression was achieved with virus produced in Lenti-X 293T cells (Takara) using psPAX2 (Addgene, #12260) and pMD2.g (Addgene, #12259) as packaging vectors and GeneJuice (Merck Milipore, 70967) as transfection reagent following the manufacturers' instructions. Constructs for lentiviral overexpression were cloned from SDOS-Myc expressing vector (Origene, RC202638) into pLenti4V5/DEST Gateway Cloning Vector using SpeI and MluI. Control vector were generated by the same procedure using the empty pCMV6-Entry vector (Origene, PS100001). Viral supernatants were concentrated using the Lenti-X™ Concentrator (Takara, PT4421-2) and resuspended to match a 40x concentrate. HUVECs were transduced with lentivirus at a final concentration of 1x. Expression was determined experimentally by qPCR to ensure comparable expression of constructs between samples.

Transgenic Mice.
Transgenic mice were generated were generated by diploid morula aggregation of knock out transgenic cZfp292 mESC cells as described in [12]. SWISS mice (Janvier) were used as wild-type donor of morula stage embryos and as transgenic recipient host (as foster mothers for transgenic mutant embryos). Offspring was confirmed to be *cZfp292*$^{-/-}$ by their fur color agouti and genotyping and backcrossed to C57Bl/6J mice (Janiver). All animal procedures were conducted as approved by local authorities (RP Darmstadt) under the license numbers FU/1064.

Animal Experiments.
Animal experiments were carried out in accordance with the principles of laboratory animal care as well as according to the German national laws. The studies have been approved by the local ethic committee (Regierungspräsidium Darmstadt, Hessen). For analysis of the aortic endothelium, aortas were dissected, en face prepared and stained according to the protocol published by Kyung et al.[13] though fixation was reduced to 2% formaldehyde/PBS for 3 min. Animals used for the analysis of the aortic endothelium were between 12-20 weeks of age and included animals of both genders. For analysis of retinal blood vessel growth, retinas were prepared from postnatal d7 pups as described previously[14]. All animals were harvested and samples were processed and imaged randomly by personal unaware of the respective genotype.

Statistical Analysis.
The ChemiDoc system (Biorad) was used for acquisition of gel and immunoblot data and ImageJ 1.52p was used for image processing. Data were analysed in Microsoft Excel 2011, GraphPad Prism 5 and Volocity. Data is shown as mean+SEM with individual data points. Data was checked for normality using the Shapiro-Wilk normality test with a threshold of 0.05. P-values were obtained using Student's two-tailed t-test or Kolmogorov-Smirnov test and are reported in the figure legends. Multiple-testing corrections were performed using the Bonferroni-Holm method as stated in the figure legends. Experiments shown in Online Figure IIIE are representative of one experiment. All other data were derived from more biological independent replicates, exact *n* are reported in the figure or the figure legends.

RESULTS

In order to identify locus-conserved endothelial intronic circRNA, we used published endothelial RNA-sequencing data with circRNAs listed in the circATLAS database (**Online Figure IA**). We first selected circRNAs commonly expressed between different types of human endothelial cells resulting in 1228 circRNAs from 868 host genes (**Fig 1A**). Further comparison of these circRNAs for their stability towards exonuclease digestion using an additional RNA sequencing dataset of RNase R-treated endothelial cells, showed that 1158 (~95%) can be considered true circRNA (**Fig. 1B**). However, only 29 of these were back-spliced to intronic cassettes (**Fig. 1C**). Importantly, 21 of the 29 candidates were also included in the top30 consistently detected human intronic circRNAs of the respective loci (**Fig. 1D**) consolidating their presence in human samples. When we additionally analysed the respective loci in mouse, several intronic circRNAs were commonly detected in circATLAS database (**Fig. 1E;** overlap of 13 host genes when comparing **Fig. 1D and 1E**), but only few circRNAs shared synteny. Of these candidates, we validated the expression and exonuclease resistance of the circRNAs cZNF292 (hsa-ZNF292_0014) and cFOXP1 (hsa-FOXP1_0045), which were both locus-conserved between human and mice (**Online Figure IB-D**). Although both were detectable, cZNF292 was expressed at higher levels. Therefore, we chose the highly and commonly expressed *cZNF292* and its locus-conserved mouse orthologue *cZfp292* (mmu-Zfp292_0007) (**Fig. 1F**) as the prime candidate for functional validation.
cZNF292 was previously described as hypoxia-inducible circRNA in endothelial cells[5]. Silencing of cZNF292 reduced proliferation and endothelial cell sprouting in culture[5] but the *in vivo* functions and mechanism of action was unknown.

The mouse orthologue *cZfp292* is resistant to exonuclease digestion and also lacks polyadenylation (**Fig. 2A/B**). To test whether removal of the retained intronic cassette leads to a loss of *cZfp292* without affecting linear *Zfp292* mRNA, we genetically deleted this region in the immortalized murine endothelial cell line H5V using the CRISPR/Cas9 system (**Fig. 2C**). Indeed, *cZfp292* was specifically deleted in several independent exon 1A deletion clones (**Fig. 2D**). Therefore, we generated *cZfp292* mutant mice by the same strategy (**Fig. 2C**). As expected, mice harboring this mutation in the germline (**Fig. 2E**) lacked the circular form *cZfp292* while the levels of the linear host gene *Zfp292* mRNA and *Zfp292* protein were unaltered (**Fig. 2F, Online Figure IIA,B**). Homozygous mutants were born at the expected Mendelian ratios and no gross abnormalities were observed during postnatal development. Furthermore, when we analyzed angiogenic vascular growth in the postnatal retina of these mice, we did not detect significant perturbations in angiogenic sprouting (**Fig. 3A/B**). However, aortic sprout outgrowth was significantly impaired in cZfp292 mutant mice compared to wildtype controls (**Fig. 3C/D**). *cZfp292*-deficient endothelial cells from the largest arterial vessel – the thoracic aorta –, revealed an altered flow morphology (**Fig. 3E/F, Online Figure II C-D**). Interestingly, RNA sequencing data and qPCR measurements indicated higher *cZNF292* levels in arterial endothelial cells compared to microvascular cells and other cells of the vascular bed (**Online Figure IIF/G**), which may underlie the observed phenotypic differences.

Next, we aimed to determine whether *cZNF292*/*cZfp292* is involved in flow-sensing and to explore the mechanism how *cZNF292* affects cell morphology. Since *cZNF292* was not detectable in HUVEC Ago-HITS-CLIP datasets and we did not find evidence for translation of these transcripts[5], we hypothesized that *cZNF292*/*cZfp292* interacts with proteins in endothelial cells. To test this hypothesis, human endothelial cell extracts were treated with or without protease K and protein complexes were separated by size using gradient ultracentrifugation (**Online Figure IIIA**). Protease treatment shifted *cZNF292* to fractions of a lighter weight (**Online Figure IIIB/C**) suggesting that it associates with a protein or a protein complex. To identify the proteins that specifically interact with *cZNF292*, we performed RNA-affinity purification using anti-sense oligonucleotides against the exon 1A for pull down, and digested contaminating linear RNA by exonucleases. Using this approach, *cZNF292* but not the linear *ZNF292* RNA was enriched (**Fig. 4A/B**). Mass-spectrometry analysis of the RNA-affinity purifications

identified 75 proteins, of which 15 were enriched more than 10-fold after *cZNF292* affinity selection (**Fig. 4C**).

The significantly enriched protein SDOS (also named Syndesmos or NUDT16L1) is an RNA binding protein, known to control focal-adhesion signalling and actin cytoskeletal reorganisation[15]. SDOS interacts with the cytoplasmic domain of Syndecan-4 (SDC4) [15,16] and binds to the focal adhesion adaptor protein paxillin (PXN) [15,17]. Interestingly, Syndecan-4 (Sdc4)-deficient mice display poorly aligned endothelial cells in the direction of flow[18], very similar to what we found in *cZfp292*$^{-/-}$ mice. We first verified the interaction of *cZNF292* with endogenous SDOS in cZNF292 pulldown samples obtained from HUVEC (**Fig. 4D**) as well as by immunoprecipitation showing that Myc-tagged SDOS specifically binds *cZNF292/cZfp292* but not the linear host RNA in HeLa or H5V cells respectively (**Fig. 4E-G, Online Figure IIIE**). The *cZNF292*-SDOS interaction was recapitulated with recombinant *cZNF292* and purified Myc-tagged SDOS *in vitro* (**Online Figure IIID/F**).

To address a functional link between *SDC4*, *SDOS*, and *cZNF292*, we separately silenced the expression of each factor and assessed endothelial cell functions and morphology (**Online Figure IVA**). We noticed that 48h post silencing, the typical "cobble-stone"-like phenotype of cultured endothelial cells started to change and adopt a more activated morphology under static conditions (**Fig. 5A**). These morphological changes were even more striking under conditions of flow (**Fig. 5A**). Here, endothelial cells lacking cZNF292, SDOS or SDC4 were resistant to unidirectional flow-induced alignment and reorganization of cytoskeletal filaments and focal adhesion complexes (**Fig 5**). In detail, silenced endothelial cells did not align in parallel to the direction of flow and showed a random angle of orientation (**Fig. 5B, Online Figure IVB-D**). The flow–induced increase in actin fiber length was significantly reduced by cZNF292, SDOS or SDC4 silencing (**Fig. 5A/C**). Moreover, silenced endothelial cells failed to remodel focal adhesions in response to laminar flow (**Fig. 5D-F**). Overall, focal adhesions show a reduction in number but an increase in size in laminar flow-exposed cZNF292, SDOS or SDC4 silenced endothelial cells compared to scrambled controls (**Fig. 5E/F**). Together these data demonstrate that silencing of *cZNF292* affects endothelial cell morphology and prevents flow induced fiber formation and focal adhesions, which is recapitulated by knocking out its binding partner *SDOS* or the up-stream transmembrane proteoglycan *SDC4*.

To understand the specificity of the circRNA-protein complex, we next determined the sites within *cZNF292* that bind to SDOS. A recent study showed that SDOS preferentially binds to C-rich sequences most commonly containing a CCCA/G motif[19]. Both *cZNF292* and *cZfp292* contain three of such putative SDOS binding sites in close proximity to the back-splice site (**Fig. 6A/B**). Two of these sites are located in exon 4 and circRNA specific exon 1A contains an additional site. Mouse cZfp292 contains one additional site in exon 1A (**Fig. 6B**). To quantify the interaction strength between SDOS and *cZNF292*, we first analysed the binding capacity of sequences surrounding the back-splice site on exon 4, exon 1A and exon 4 and the full length *cZNF292* sequence for their binding capacity with recombinant SDOS by electrophoretic mobility shift assays (**Fig. 6C/D**). SDOS was bound with a higher affinity (dissociation constant, K_D: 161 nM) to oligonucleotides covering the full back spliced region compared to exon 4 alone (K_D: 548 nM), but similar to exon 1A and exon 4 (K_D: 288 nM) (**Fig. 6C**). We also validated binding of the predicted sequence motives to SDOS (**Fig. 6E**). Importantly, mutation of the respective motives led to reduced binding between the cZNF292 sequences and SDOS, but did not fully prevent the interaction at high SDOS concentrations (**Online Figure VA)**. Of note, lentiviral overexpression of cZNF292 with mutated binding sites recapitulated the effects observed by silencing of cZNF292 (**Online Figure VB-F**).

Based on these data, we suggest that monomers of the SDOS dimer can bind single motives in the context of the large RNA with multiple binding motifs. Thus, the enhanced affinity resembles avidity compared to individual binding motifs.

To identify the interaction sites in SDOS, we compared the crystal structures of SDOS[16] with published RNA interaction models of its family member NUDT16 and found four residues (H29, R55, F66, E138) that appear critical for RNA-binding of SDOS (**Fig. 7A**). Therefore, we mutated the respective residues to alanine and tested the interaction of the mutant with cZNF292 by RNA immunoprecipitation (RIP) (**Fig. 7B/C**) and EMSA experiments (**Fig. 7D**). Indeed, the SDOS mutants showed a significantly diminished *cZNF292* binding activity in both assays (**Fig. 7B-D**).

To determine to what extend the interaction of *cZNF292* and SDOS contributes to the observed morphological phenotype, we overexpressed a SDOS mutant lacking the *cZNF292* interaction sites (**Fig. 8A, Online Figure VIA**). Lentiviral overexpression of the SDOS 4x Ala mutant but not the wild-type protein prevented flow induced cell alignments and PXN relocation (**Fig. 8B-D, Online Figure VIB-D**) with a very similar phenotype as shown before for silencing of cZNF292 (**Fig. 5**). These data, demonstrate that blocking interaction of *cZNF292* with SDOS is sufficient to prevent morphological flow-responses in endothelial cells.

These results suggest a model whereby cZNF292 enhances SDC4-SDOS interaction and subsequent signaling. To test this model, we determined the effect of cZNF292 overexpression of SDC4-SDOS protein interaction by co-immunoprecipitation. Overexpression of cZNF292 indeed increased the binding of SDC4 to SDOS (**Fig. 8E/F**).

Conclusions.

In summary, we show a new approach to determine targetable circRNAs for *in vivo* characterization and demonstrate that the circRNA *cZNF292* interacts with SDOS to regulate endothelial flow responses *in vitro* and *in vivo*. It is well established that endothelial cells respond to flow by aligning in the direction of (unidirectional) flow through the reorganization of cytoskeletal filaments and focal adhesion complexes. This crucial adaptive response maintains the anti-inflammatory and atheroprotective properties of the endothelial cell monolayer. Interestingly, we now found that cZNF292/cZfp292 is required for the morphological adaptations of endothelial cells to laminar flow *in vitro* and *in vivo*. *cZNF292*/*cZfp292* deficiency thereby recapitulated several known effects of *SDC4* knockouts[18,20], suggesting that *cZNF292*/*cZfp292* act down-stream of SDC4 by influencing the signaling of SDOS and PXN. SDC4 has been proposed as pro-angiogenic molecule *in vitro* [21], but physiological retinal angiogenesis was not disturbed in *Sdc4*$^{-/-}$ mice[22]. Similarly, we previously found cZNF292 silencing to impair angiogenic sprouting in spheroid assays *in vitro*[5], whereas cZfp292 deficiency *in vivo* only resulted in minor alterations of retinal angiogenesis. The difference between the *in vitro* and *in vivo* studies may be due to the differences in the multidimensional environment which endothelial cells face. Examples include variances in mechanical forces, which profoundly influence endothelial cell focal adhesions and signalling. Interestingly, we show that outgrowth of aortic endothelial cells, which show highest expression levels of cZNF292 in the vascular bed, was prevented in *cZfp292-/-* mice suggesting that aortic endothelial cells are preferentially affected by the lack of *cZfp292*. Nevertheless, further studies will need to dissect to which extent the expression of *cZfp292* in other cell types contributes to the observed phenotype. Our study is additionally limited by the sole observation of the phenotype under baseline conditions and the unknown function of cZNF292 in humans. It will be important to assess how cZfp292 may influence the morphology and function of endothelial cells in pro-atherosclerotic or under other stress conditions.

Our study further demonstrates that *cZNF292* directly interacts with SDOS thereby controlling PXN distribution and focal adhesion formation. We have mapped the interaction sites and demonstrate that SDOS binding sites located around the back-splice site are required for the interaction. Importantly, reduction of *cZNF292* or mutation of SDOS-*cZNF292* interaction sites prevented the morphological adaptation of endothelial cells to flow. Given the known interaction between SDOS with both SDC4[15,16]

and PXN[17], our data therefore supports a model in which *cZNF292* binds to SDOS to co-mediate SDC4 signalling to PXN, ultimately modulating focal adhesions formation. This model is further supported by the finding that overexpression of cZNF292 augments the interaction of SDOS with SDC4. However, it should be noted that the protein interactions of cZNF292 might not be limited to SDOS given the enrichment of various other proteins following cZNF292 pulldown.

In summary, this study reports that a circRNA acts as a regulator of flow responses in endothelial cells by its interaction with a protein. Only recently, two studies reported first insights into the control of endothelial barrier function and adherens junctions by long non-coding RNAs[23,24]. Our study is the first to show a regulatory role of a circRNA, acting as scaffolding component in the fine-tuned cytoskeletal response of endothelial cells to flow.

ACKNOWLEDGMENT
We would like to thank Tobias Jakobi and Nicole Ritter for technical assistance.

SOURCES OF FUNDING
This study was supported by the ERC (Advanced grant Angiolnc) to S.D. and by the Deutsche Forschungsgemeinschaft (DFG, German Research Foundation) - Project-ID 403584255 - TRR 267 to P.G., T.B., I.W., M.S. and S.D; Research in the Potente laboratory was supported by the ERC (Consolidator Grant EMERGE) and the Foundation Leducq Transatlantic Network

DISCLOSURE
None.

AUTHORSHIP CONTRIBUTIONS
Conceptualization: A.W.H., N.J., S.D; Experimental design: A.W.H, A.N.J., A.M., M.P., T.B., P.G., N.J., M.S., S.D.; Experimental investigations: A.W.H, A.J.N, A.M., M.K., C.S., I.W., C.D., A.F., M.M.R., P.G. G.B.; Writing – original draft preparation: A.W.H., S.D.; Funding acquisition: M.P., T.B., P.G., I.W., M.S., S.D.; All authors revised the manuscript.

SUPPLEMENTAL MATERIALS
Expanded Material & Methods
Online Figures I – VI
References 25-30

REFERENCES

1. Chiu JJ, Chien S. Effects of disturbed flow on vascular endothelium: pathophysiological basis and clinical perspectives. *Physiol Rev*. 2011;91:327–387.
2. Baeyens N, Schwartz MA. Biomechanics of vascular mechanosensation and remodeling. *Mol Biol Cell*. 2016;27:7–11.
3. Jaé N, Dimmeler S. Noncoding RNAs in Vascular Diseases. *Circ Res*. 2020;126:1127–1145.
4. Glazar P, Papavasileiou P, Rajewsky N. circBase: a database for circular RNAs. *RNA*. 2014;20:1666–1670.
5. Boeckel J-N, Jaé N, Heumüller AW, Chen W, Boon RA, Stellos K, Zeiher AM, John D, Uchida S, Dimmeler S. Identification and Characterization of Hypoxia-Regulated Endothelial Circular RNA. *Circ Res* [Internet]. 2015;117:884–90. Available from: http://www.ncbi.nlm.nih.gov/pubmed/26377962
6. Shan K, Liu C, Liu B-H, Chen X, Dong R, Liu X, Zhang Y-Y, Liu B, Zhang S-J, Wang J-J, Zhang S-H, Wu J-H, Zhao C, Yan B. Circular Noncoding RNA HIPK3 Mediates Retinal Vascular Dysfunction in Diabetes Mellitus. *Circulation*. 2017;136:1629–1642.
7. Piwecka M, Glažar P, Hernandez-Miranda LR, Memczak S, Wolf SA, Rybak-Wolf A, Filipchyk A, Klironomos F, Cerda Jara CA, Fenske P, Trimbuch T, Zywitza V, Plass M, Schreyer L, Ayoub S, Kocks C, Kühn R, Rosenmund C, Birchmeier C, Rajewsky N. Loss of a mammalian circular RNA locus causes miRNA deregulation and affects brain function. *Science* [Internet]. 2017;357. Available from: http://www.ncbi.nlm.nih.gov/pubmed/28798046
8. Xia P, Wang S, Ye B, Du Y, Li C, Xiong Z, Qu Y, Fan Z. A Circular RNA Protects Dormant Hematopoietic Stem Cells from DNA Sensor cGAS-Mediated Exhaustion. *Immunity*. 2018;48:688–701.e7.
9. Pamudurti NR, Patop IL, Krishnamoorthy A, Ashwal-Fluss R, Bartok O, Kadener S. An in vivo strategy for knockdown of circular RNAs. *Cell Discov* [Internet]. 2020;6:52. Available from: http://www.ncbi.nlm.nih.gov/pubmed/32818061
10. Zheng Q, Bao C, Guo W, Li S, Chen J, Chen B, Luo Y, Lyu D, Li Y, Shi G, Liang L, Gu J, He X, Huang S. Circular RNA profiling reveals an abundant circHIPK3 that regulates cell growth by sponging multiple miRNAs. *Nat Commun*. 2016;7:11215.
11. Jakobi T, Siede D, Eschenbach J, Heumüller AW, Busch M, Nietsch R, Meder B, Most P, Dimmeler S, Backs J, Katus HA, Dieterich C. Deep Characterization of Circular RNAs from Human Cardiovascular Cell Models and Cardiac Tissue. *Cells*. 2020;9.
12. Ritter N, Ali T, Kopitchinski N, Schuster P, Beisaw A, Hendrix DA, Schulz MH, Müller-McNicoll M, Dimmeler S, Grote P. The lncRNA Locus Handsdown Regulates Cardiac Gene Programs and Is Essential for Early Mouse Development. *Dev Cell*. 2019;50:644–657.e8.
13. Ko KA, Fujiwara K, Krishnan S, Abe J-I. En Face Preparation of Mouse Blood Vessels. *J Vis Exp*. 2017;
14. Lim R, Sugino T, Nolte H, Andrade J, Zimmermann B, Shi C, Doddaballapur A, Ong YT, Wilhelm K, Fasse JWD, Ernst A, Kaulich M, Husnjak K, Boettger T, Guenther S, Braun T, Krüger M, Benedito R, Dikic I, Potente M. Deubiquitinase USP10 regulates Notch signaling in the endothelium. *Science*. 2019;364:188–193.
15. Baciu PC, Saoncella S, Lee SH, Denhez F, Leuthardt D, Goetinck PF. Syndesmos, a protein that interacts with the cytoplasmic domain of syndecan-4, mediates cell spreading and actin cytoskeletal organization. *J Cell Sci*. 2000;113 Pt 2:315–324.
16. Kim H, Yoo J, Lee I, Kang YJ, Cho H-S, Lee W. Crystal structure of syndesmos and its interaction with Syndecan-4 proteoglycan. *Biochem Biophys Res Commun*. 2015;463:762–767.
17. Denhez F, Wilcox-Adelman SA, Baciu PC, Saoncella S, Lee S, French B, Neveu W, Goetinck PF. Syndesmos, a syndecan-4 cytoplasmic domain interactor, binds to the focal adhesion adaptor proteins paxillin and Hic-5. *J Biol Chem*. 2002;277:12270–12274.
18. Baeyens N, Mulligan-Kehoe MJ, Corti F, Simon DD, Ross TD, Rhodes JM, Wang TZ, Mejean CO, Simons M, Humphrey J, Schwartz MA. Syndecan 4 is required for endothelial alignment in

flow and atheroprotective signaling. *Proc Natl Acad Sci U S A*. 2014;111:17308–17313.
19. Avolio R, Järvelin AI, Mohammed S, Agliarulo I, Condelli V, Zoppoli P, Calice G, Sarnataro D, Bechara E, Tartaglia GG, Landriscina M, Castello A, Esposito F, Matassa DS. Protein Syndesmos is a novel RNA-binding protein that regulates primary cilia formation. *Nucleic Acids Res*. 2018;46:12067–12086.
20. Vuong TT, Reine TM, Sudworth A, Jenssen TG, Kolset SO. Syndecan-4 is a major syndecan in primary human endothelial cells in vitro, modulated by inflammatory stimuli and involved in wound healing. *J Histochem Cytochem Off J Histochem Soc*. 2015;63:280–292.
21. Echtermeyer F, Streit M, Wilcox-Adelman S, Saoncella S, Denhez F, Detmar M, Goetinck P. Delayed wound repair and impaired angiogenesis in mice lacking syndecan-4. *J Clin Invest*. 2001;107:R9–R14.
22. Corti F, Wang Y, Rhodes JM, Atri D, Archer-Hartmann S, Zhang J, Zhuang ZW, Chen D, Wang T, Wang Z, Azadi P, Simons M. N-terminal syndecan-2 domain selectively enhances 6-O heparan sulfate chains sulfation and promotes VEGFA(165)-dependent neovascularization. *Nat Commun*. 2019;10:1562.
23. Stanicek L, Lozano-Vidal N, Bink DI, Hooglugt A, Yao W, Wittig I, van Rijssel J, van Buul JD, van Bergen A, Klems A, Ramms AS, Le Noble F, Hofmann P, Szulcek R, Wang S, Offermanns S, Ercanoglu MS, Kwon H-B, Stainier D, Huveneers S, Kurian L, Dimmeler S, Boon RA. Long non-coding RNA LASSIE regulates shear stress sensing and endothelial barrier function. *Commun Biol*. 2020;3:265.
24. Lyu Q, Xu S, Lyu Y, Choi M, Christie CK, Slivano OJ, Rahman A, Jin Z-G, Long X, Xu Y, Miano JM. SENCR stabilizes vascular endothelial cell adherens junctions through interaction with CKAP4. *Proc Natl Acad Sci U S A*. 2019;116:546–555.
25. Rappsilber J, Mann M, Ishihama Y. Protocol for micro-purification, enrichment, pre-fractionation and storage of peptides for proteomics using StageTips. *Nat Protoc*. 2007;2:1896–1906.
26. Olsen J V, de Godoy LMF, Li G, Macek B, Mortensen P, Pesch R, Makarov A, Lange O, Horning S, Mann M. Parts per million mass accuracy on an Orbitrap mass spectrometer via lock mass injection into a C-trap. *Mol Cell Proteomics*. 2005;4:2010–2021.
27. Cox J, Mann M. MaxQuant enables high peptide identification rates, individualized p.p.b.-range mass accuracies and proteome-wide protein quantification. *Nat Biotechnol*. 2008;26:1367–1372.
28. Tyanova S, Temu T, Sinitcyn P, Carlson A, Hein MY, Geiger T, Mann M, Cox J. The Perseus computational platform for comprehensive analysis of (prote)omics data. *Nat Methods*. 2016;13:731–740.
29. Trésaugues L, Lundbäck T, Welin M, Flodin S, Nyman T, Silvander C, Gräslund S, Nordlund P. Structural Basis for the Specificity of Human NUDT16 and Its Regulation by Inosine Monophosphate. *PLoS One*. 2015;10:e0131507.
30. Jost I, Shalamova LA, Gerresheim GK, Niepmann M, Bindereif A, Rossbach O. Functional sequestration of microRNA-122 from Hepatitis C Virus by circular RNA sponges. *RNA Biol*. 2018;15:1032–1039.

FIGURE LEGENDS

Fig.1 Intron-containing circRNA screening. A, Venn diagrams showing commonly expressed circRNAs in different endothelial RNA sequencing datasets (HUVEC: human umbilical vein endothelial cells, HAoEC: human aortic endothelial cells, HCMEC: human cardiac microvascular endothelial cells). The threshold for counting a circRNA as expressed was set to the detection of at least two reads in at least two samples. **B,** Overlap between endothelial common circRNA and their detection by RNA-seq of exonuclease RNase R treated HUVEC RNA. **C,** Intronic-spliced circRNA of the selection shown in A/B ranked by their circular-to-linear expression ratio in HUVECs. **D,** Top 30 of 1404 human intronic circRNAs of the genesubset shown in C listed in the circATLAS database and sorted by detection rate. **E,** Top30 of 302 murine intronic circRNAs of the genesubset shown in C mice listed in the circATLAS database and sorted by detection rate. **F,** Human and (inverted) mouse ZNF292/Zfp292 locus with conserved circRNA isoforms.

Fig.2 cZfp292 is specifically depletable in vivo. **A,** qRT-PCR measuring RNA levels in HUVEC cell lysates after exonuclease digestion or mock treatment (n=3) or **B,** following Poly-dT fractionation (n=4) of H5V cells. **C,** Scheme depicting the exon1A knockout strategy. **D,** qRT-PCR measurements of circular and linear Zfp292 RNA levels after exon1A deletion and clonal propagation in H5V cells. Representative gel images showing deletion of cZfp292 on **E,** DNA level in tail biopsies and **F,** RNA level in liver tissue samples of cZfp292 wildtype or mutant mice. Data is depicted as mean±SEM, statistical analysis by two-sided unpaired student's t-test (*) a value of $p<0.05$ is considered significant.

Fig.3 cZfp292 alters endothelial morphology in vivo. **A/B,** Representative image and quantification of postnatal d7 retina outgrowth in cZfp292-/- mice compared to wildtype littermates (samples were stained using the endothelial markers CD31 shown in cyan and ERG shown in red). **C/D,** Representative images and quantification of aortic ring sprout outgrowth after 7 days of culture in the presence of 30ng/ml VEGF-A. Mean values are representative of 4 technical replicates. **E/F,** Images and cell shape quantification of *en face* stained aorta sections showing ECs by CD144 and CD31 staining (n=4). White scale bar equals 200µm, yellow scale bar equals 100 µm, red scale bar equals 20µm. Data is depicted as mean±SEM, statistical analysis by two-sided unpaired student's t-test (*), a value of $p<0.05$ is considered significant.

Fig.4 cZNF292 interacts with SDOS. A/B, Recovery of circular/linear ZNF292 RNA measured by qRT-PCR after RNA-pulldown using biotinylated-antisense-probes targeting the circRNA specific exon1A in HUVEC cell lysates under native conditions (n=8). **C,** Volcano plot depicting LC-MS-identified proteins after cZNF292-pulldown in HUVECs (n=8). **D,** Immunoblot showing recovery of endogenous SDOS following native cZNF292-pulldown in HUVEC lysates (n=1). **E,** Representative immunoblot and **F,** gel images of recovered SDOS-myc and cZNF292 after overexpression of SDOS-myc and immunoprecipitation in HeLa, quantification shown in **G** (n=4). Data is depicted as mean±SEM, statistical analysis by two-sided unpaired student's t-test (*) or Kolmogorov-Smirnoff test (#), a value of $p<0.05$ is considered significant.

Fig.5 cZNF292 and SDOS silencing prevent cytoskeletal remodeling in response to laminar flow. A, Representative images of HUVECs after siRNA silencing and exposure to laminar flow stained for actin fibers by phalloidin (green) and the focal adhesion marker Paxillin (PXN, shown in red). HUVECs were silenced with siRNA for 24h before cells were reseeded and exposed to 12 dyne laminar flow for 40h. Static controls were treated equally but were not exposed to flow. **B,** Distribution of actin fibers compared to the direction of flow in HUVECs following siRNA silencing and laminar flow (n=3). **C,** Quantification of actin fiber length following silencing of cZNF292/SDOS or SDC4 and subsequent exposure to flow (n=3). **D,** Single cell excerpts of siRNA silenced HUVECs 40h after exposure to 12 dyne laminar flow. HUVECs were stained for VE-Cadherin, Actin and PXN. **E/F,** Quantification of focal adhesions (FA)

identified by PXN staining in HUVECs following knockdown and laminar flow (in 45 cells of 3 biological replicates). White scale bar equals 100 µm, red scale bar equals 25 µm. Data is depicted as mean±SEM, statistical analysis by two-sided unpaired student's t-test (*) with Bonferroni-Holm correction or Kolmogorov-Smirnoff test (#), a value of $p<0.05$ is considered significant.

Fig.6 Molecular cZNF292/SDOS interaction analysis. **A,** Schemes depicting cZNF292 as a circle with potential SDOS binding sites (red) in close proximity to the back-splice site (blue) **B,** Schematic comparison of human and mouse cZNF292/cZfp292 sequence following pairwise sequence alignment and indicating positions of potential SDOS binding sites. **C,** EMSA depicting interaction between increasing concentrations of SDOS and equal amount of radiolabeled-RNA oligos comprising an excerpt of exon4, exon4+exon1A or the full-length cZNF292 sequence, quantification is shown in **D,** (n=2), dissociation constants were calculated using the Hills-equation. **E,** Interaction analysis between SDOS and the human SDOS motives outlined in B using EMSAs (n=3).

Fig.7 Distinct mutations disrupt cZNF292/SDOS interaction. A, Crystal structure of SDOS (PDB code 3kvh with symmetry-related molecule representing SDOS dimer) showing predicted RNA-binding residues (red/black by monomer). **B/C,** Representative images and quantification of cZNF292 levels after immunoprecipitation of wildtype or mutated overexpressed SDOS-Myc in HeLa cell lysates (n=5). **D**, Analysis of the interaction between mutated SDOS and RNA oligos comprising the SDOS bindings sites of Exon4, Exon4+Exon1A or the full length linear cZNF292 RNA sequence by electromobility shift assay (n=2).

Fig. 8 Disruption of cZNF292/SDOS interaction alters endothelial flow morphology.
A, Quantification of SDOS RNA levels by qRT-PCR 48h following lentiviral overexpression of wildtype and mutated SDOS in HUVECs (n=3). **B,** Representative Images of HUVECs following lentiviral overexpression of wildtype or mutated SDOS and 40h exposure to 12 dyne laminar flow. HUVECs were stained for actin by phalloidin (cyan) and for the focal adhesion marker paxillin (PXN, shown in magenta) **C,** Distribution of the orientation of nuclei or **D,** actin fibers compared to the direction of flow in HUVECs after lentiviral overexpression of SDOS variants and exposure to laminar flow (n=2). **E/F,** Representative image and quantification of SDC4 following immunoprecipitation of SDOS-Myc in HeLa cells (n=5). Membrane-associated fractions were extracted using a commercial kit 48h after overexpression of SDOS-Myc and SDC4-Flag in the presence of either a cZNF292 overexpression construct or a respective Mock control. Following SDOS-Myc was precipitated using antibodies targeting the Myc-tag. Immunoblots in F were stained for SDC4 (upper panel) and reprobed for SDOS-Myc. Data is depicted as mean±SEM, statistical analysis by two-sided paired student's t-test (#), a value of $p<0.05$ is considered significant.

NOVELTY AND SIGNIFICANCE

What Is Known?

- Circular RNA are generated by back splicing of genes and are expressed in high numbers in all tissues.
- Circular RNAs have been shown to interact with other RNAs or proteins to regulate cellular function. However, in vivo function is mainly unknown.

What New Information Does This Article Contribute?

- We show that deletion of the circular RNA cZfp292 in vivo affects endothelial cell function and morphology, including induction of aberrant flow alignment in the aorta.

- We characterize the mechanism by which the circular RNA cZNF292 affects endothelial cell functions showing that cZNF292 interacts with the protein Syndesmos (SDOS). This interaction allows endothelial cells to respond to mechanical activation by flow. Inhibition of this interaction by either mutation of the SDOS interaction site or the binding site in cZNF292 blocked the response to laminar flow.

- These findings provide first evidence for the control of flow responses by a circular RNA.

In this study, we show that the circular RNA cZNF292 interacts with SDOS protein and influences endothelial flow morphology. Mutations interrupting cZNF292-SDOS interactions inhibit laminar flow-induced alignment. This functionality is conserved to the murine circRNA cZfp292, where depletion of cZfp292 leads to aberrant aortic flow alignment *in vivo*. This novel example of a conserved function of a circRNA/protein interaction in cellular response to mechanical activation highlights the importance of non-coding RNA interactomes in cellular structure and function.

FIGURE 1

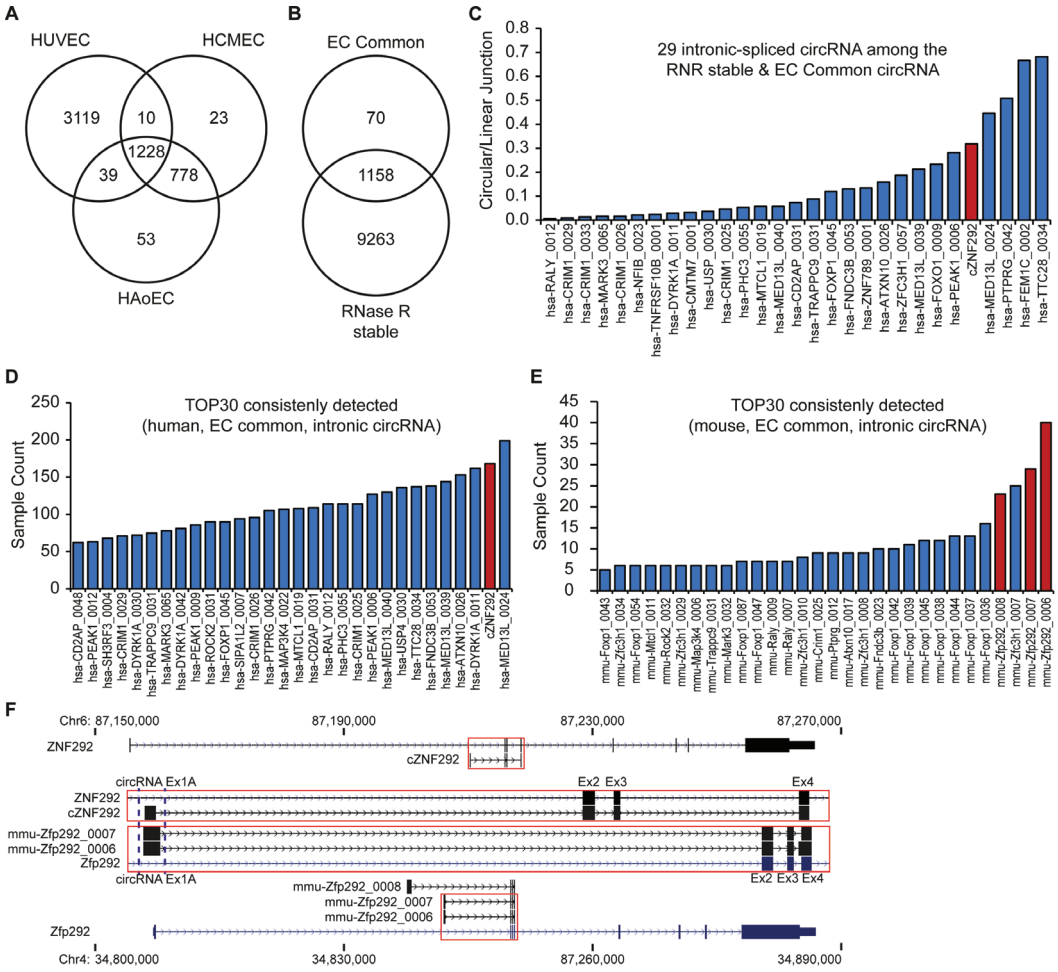

FIGURE 2

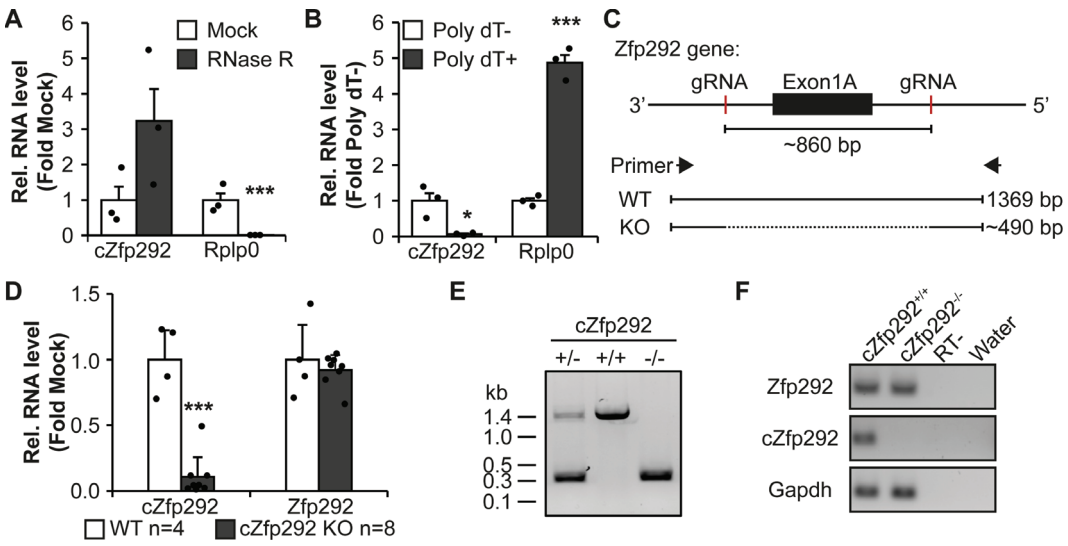

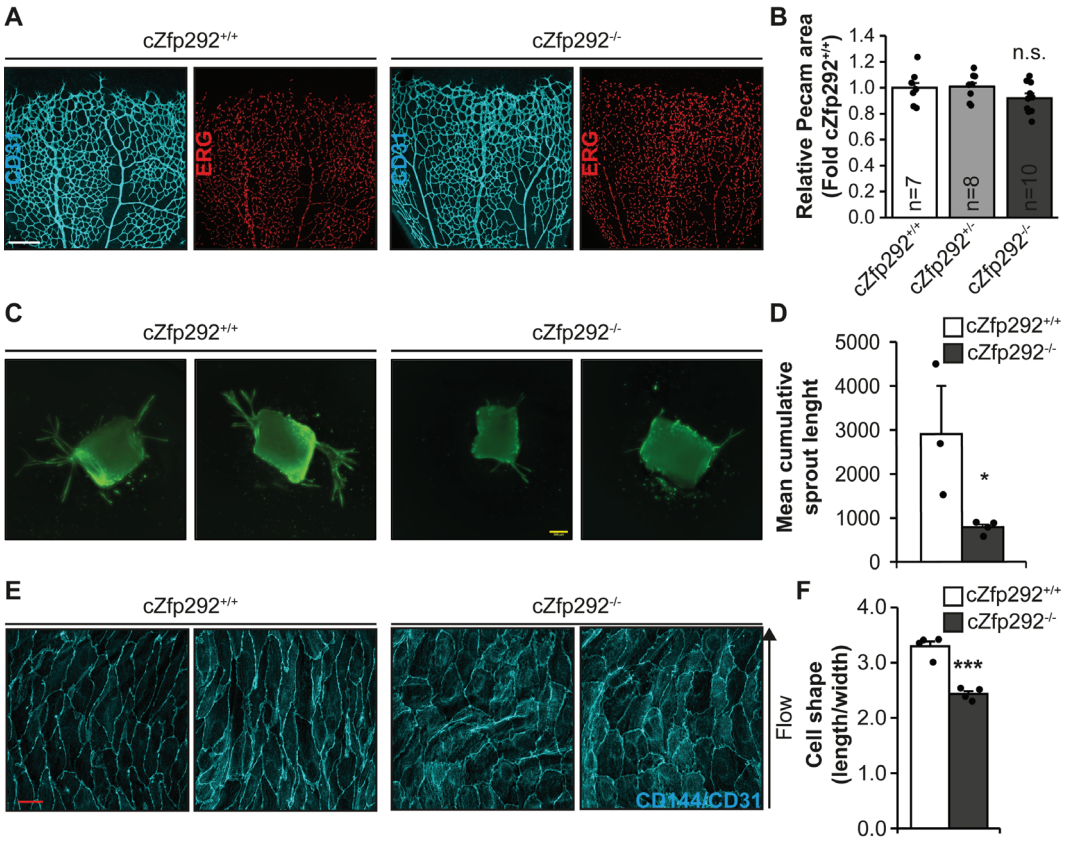

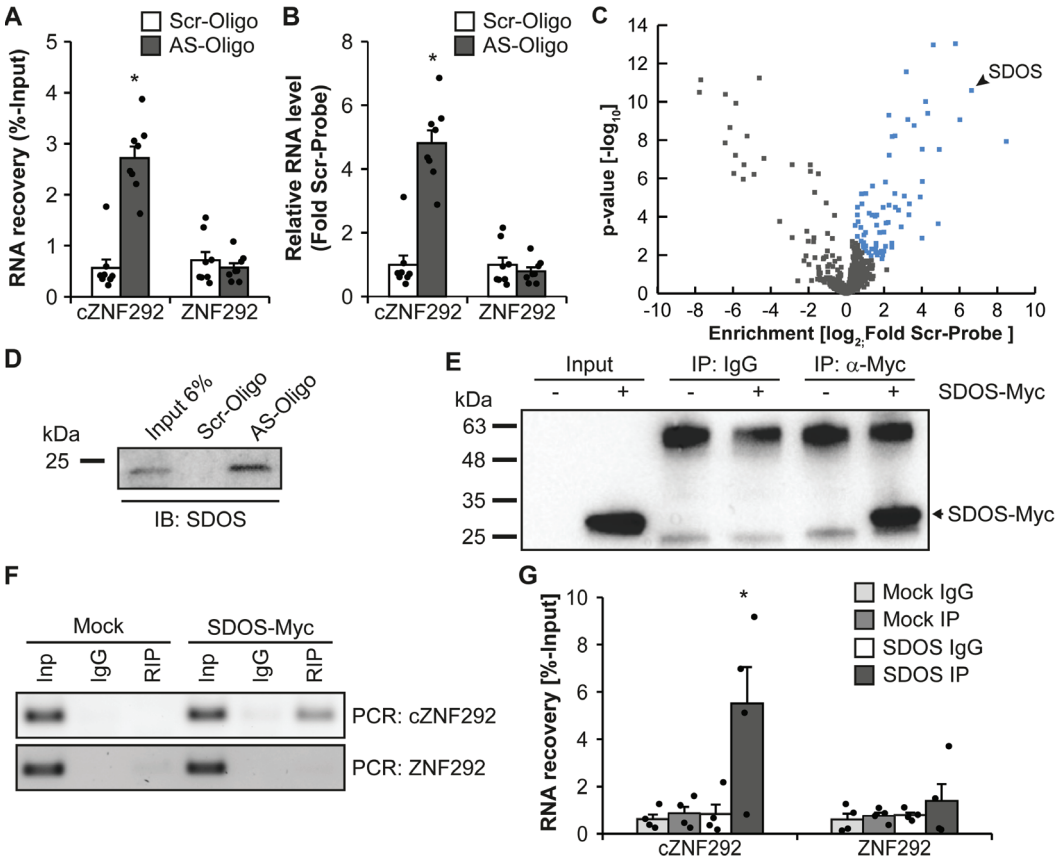

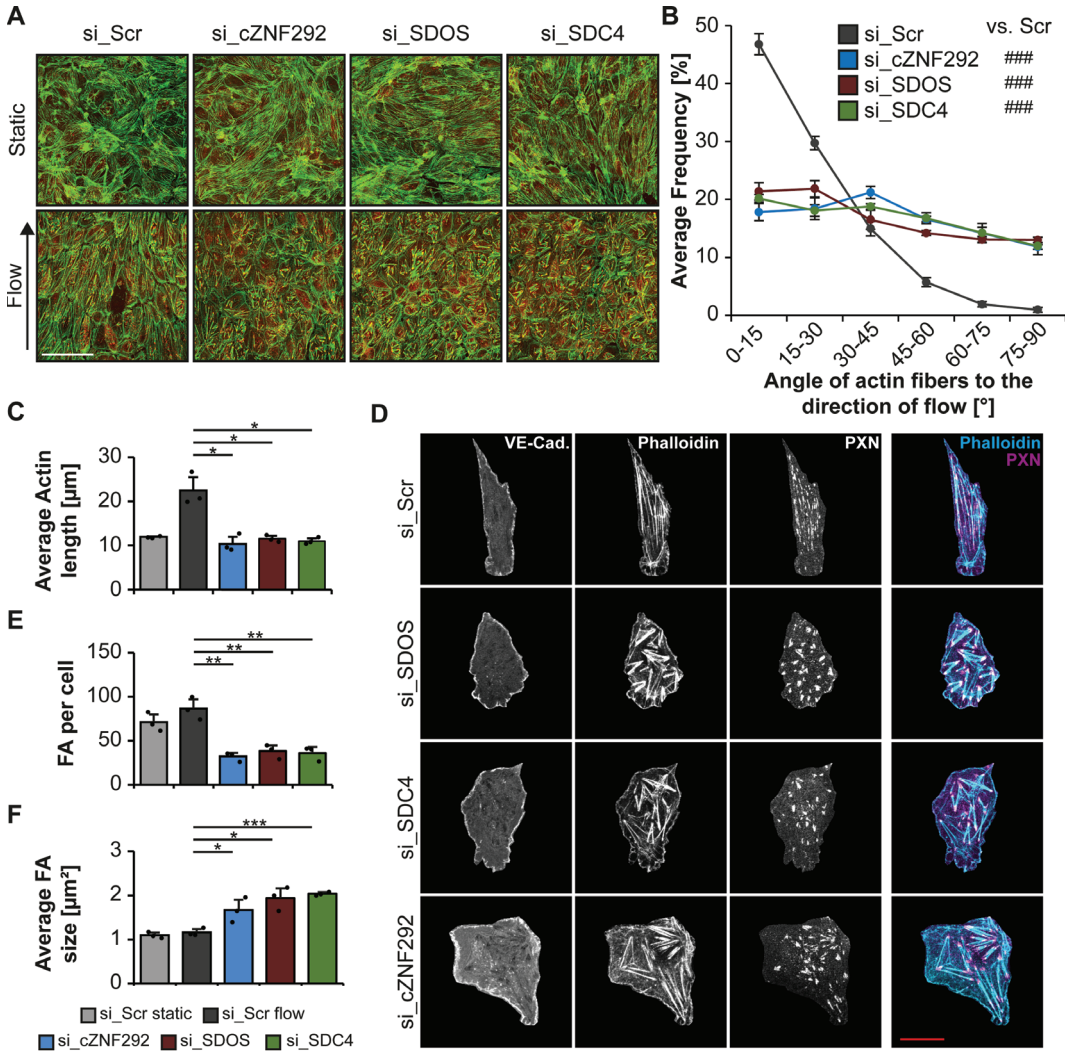

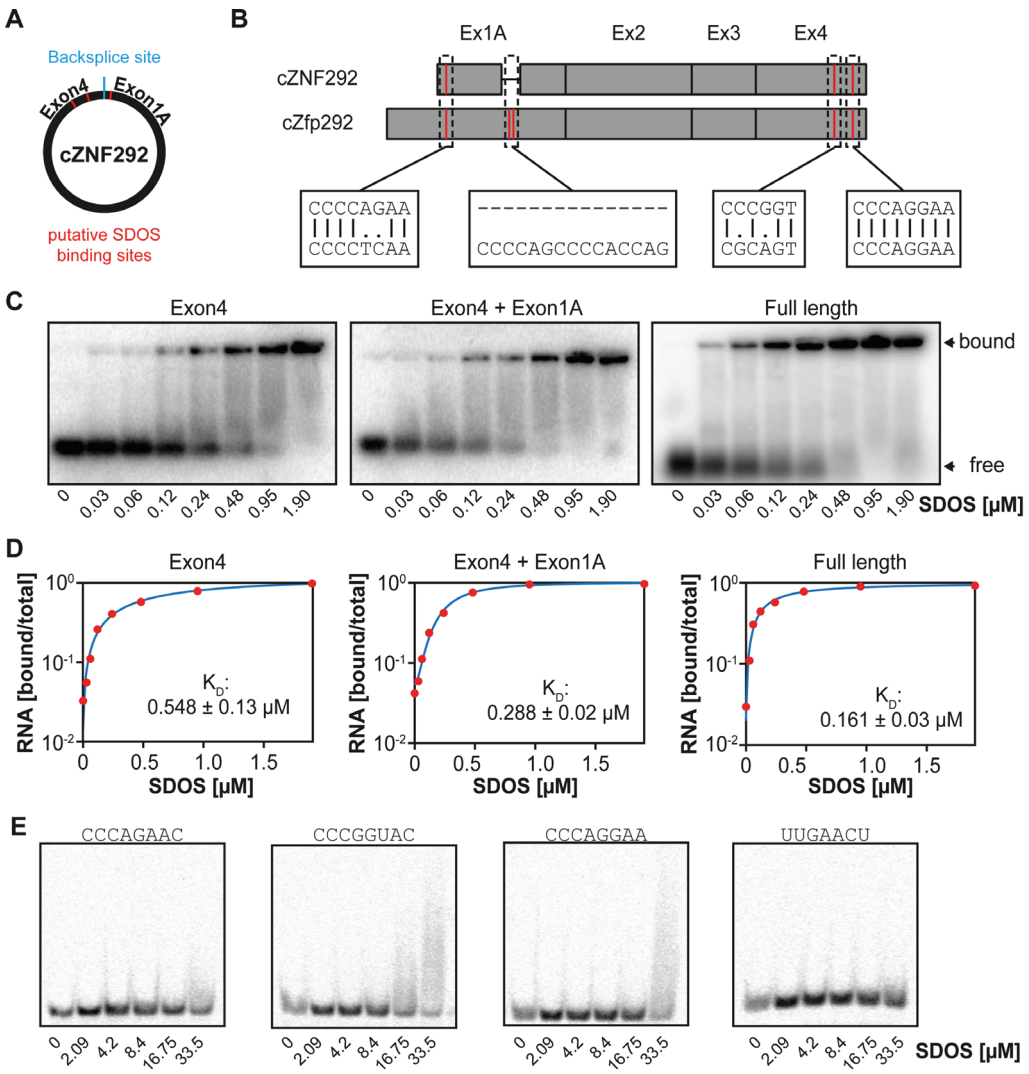

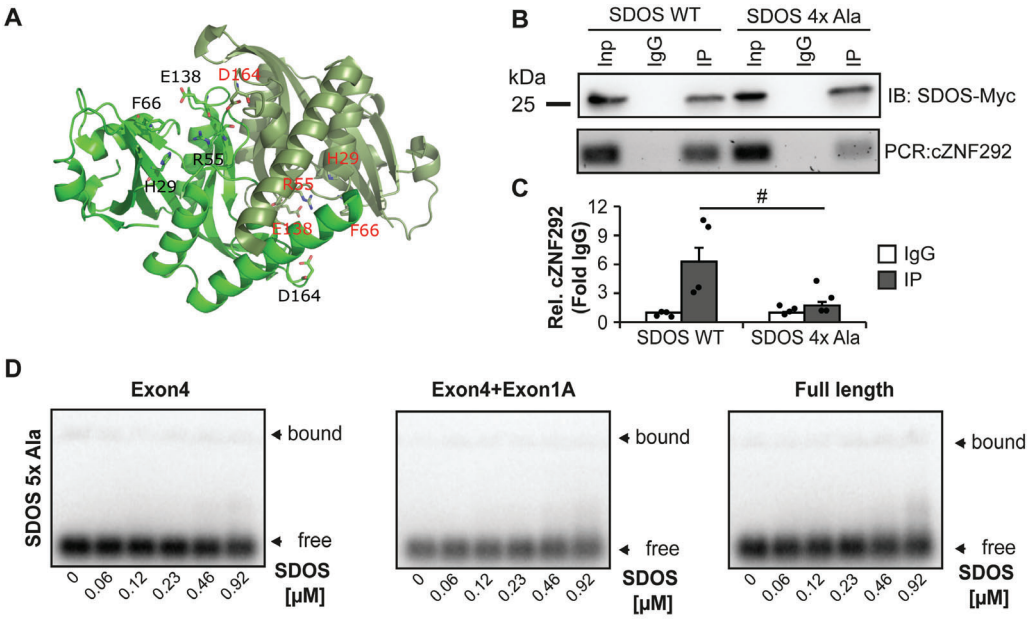

FIGURE 8